Chemical Engineering Science 326 (2026) 123611

Contents lists available at ScienceDirect

Chemical Engineering Science

journal homepage: www.elsevier.com/locate/ces

Atomistic view of green steel: simulation of early-stage direct reduction of wüstite (FeO) by hydrogen

Yushan Bu [a], Kejiang Li [a,*], Yan Ma [b], Zeng Liang [a], Jianliang Zhang [a,*], Dierk Raabe [b,*]

[a] School of Metallurgical and Ecological Engineering, University of Science and Technology Beijing, Beijing 100083, China
[b] Max Planck Institute for Sustainable Materials, Max-Planck-Straße 1, Düsseldorf 40237, Germany

ARTICLE INFO

Keywords:
Green Steel
Hydrogen reduction
FeO
Molecular dynamics
ReaxFF

ABSTRACT

Steel production accounts for about 8% of global CO_2 emissions, making it a major contributor to global warming. Direct reduction of iron ores with hydrogen offers a promising mitigation strategy. Understanding the atomistic interactions between solid oxides and hydrogen is crucial for scaling this technique to the near 2 billion-ton annual production. This study uses molecular dynamics simulations to explore the interactions of solid wüstite (FeO) with hydrogen. The redox process follows a reactive force field model (ReaxFF), revealing key atomistic dynamics and complex reactions. The results show that hydrogen dissociates into atomic form at the oxide surface, binding to the outermost oxygen ions. The oxygen content in FeO drops from 50% to 28% at the interface after 1120 ps, forming an oxygen ion gradient. Oxygen ions diffuse outward, reacting with hydrogen to form water. Hydrogen atoms migrate through FeO while maintaining a bond distance of ~1.0 Å from oxygen. Hydrogen diffusion at the solid–gas interface ranges from D = 20–200 $Å^2$/ps, while in the solid FeO, it drops to D < 5 $Å^2$/ps. Oxygen ion diffusion is significantly slower than hydrogen, making oxygen transport the rate-limiting step. These insights provide guidance for optimizing green steel production using hydrogen.

1. Introduction

The steel industry is responsible for about 8% of global CO_2 emissions or, respectively, one-third of all industrial CO_2 emissions. This qualifies steel production as the largest single contributor to global warming, thus creating an urgent decarbonization challenge (Raabe, 2023; Raabe et al., 2019). This is due to the fact that 75% of the demand for reducing agents and energy is met by fossil fuels in today's steel sector (IEA, 2022). In the next two decades, this decarbonization challenge is expected to grow owing to a further increase in the global steel demand by 20–25%. This rise is fueled by the need for more than thousand types of steel grades in construction, industrial infrastructure, transport, power plants, advanced machinery, and numerous safety–critical components. Nowadays, 70% of the global iron and steel is made via integrated blast furnaces and basic oxygen furnace production, using fossil sources as reductants and fuels, creating 80% of all CO_2 emissions in steel making. At global average this carbon-based integrated steel production route generates ~1.8 tons of CO_2 per ton of steel (Vogl et al., 2018). Therefore, renewable and carbon-lean reductants and energy sources are necessary to replace their fossil-originated counterparts. In this context, hydrogen-based extractive metallurgy is an attractive solution because its associated redox by-product is H_2O instead of CO_2, thus directly targeting the hard-to-abate part in steel production, namely, the extraction of iron from its oxides. In the realm of hydrogen-based reduction methods, solid-state direct reduction of iron oxides with hydrogen stands out as a promising and scalable option (Spreitzer and Schenk, 2019; Souza Filho et al., 2022; Sastri et al., 1982; Chen and Zuo, 2021). The natural-gas-based direct reduction technology is currently, where steam reforming is nowadays providing the Co + H_2 reductant gas mixture is well established and mature. Some of the underlying knowledge can be transferred to hydrogen-based direct reduction, and huge corresponding investments are underway around the globe (Vogl et al., 2018; IEA, 2020). Moreover, scalability is particularly relevant as forecasts anticipate a global steel demand of approximately 2.5 billion tons annually by about 2040 (Raabe, 2023; Raabe et al., 2019). Future sustainable ironmaking approaches are expected to meet such a huge demand.

Previous studies have revealed that hydrogen reduces iron oxides much faster than carbon monoxide does (Spreitzer and Schenk, 2019; El-Geassy and Nasr, 1988; Gallegos and Apecetche, 1988; Weiss et al., 2009; Zhang et al., 2016; Bonalde et al., 2005). Particularly, hydrogen offers a substantial kinetic advantage over carbon monoxide in the early

* Corresponding authors.
E-mail addresses: likejiang@ustb.edu.cn (K. Li), zhang.jianliang@hotmail.com (J. Zhang), d.raabe@mpie.de (D. Raabe).

https://doi.org/10.1016/j.ces.2026.123611
Received 11 November 2025; Received in revised form 28 January 2026; Accepted 12 February 2026
Available online 14 February 2026

stages of reducing hematite to magnetite and then to wüstite. Experimental results showed that the rate of hematite reduction by hydrogen was about two times faster than the reaction with carbon monoxide (Bonalde et al., 2005). However, this kinetic advantage diminishes in the final reduction step, i.e., from wüstite (FeO) to iron. The reduction kinetics is one order of magnitude slower than the initial hematite reduction. Thus, the reduction of wüstite to iron is considered to be the rate-limiting step (Halder and Fruehan, 2008); substantially lowering the efficiency of green steel production (Zhang et al., 2022; Meshram et al., 2023; Chen et al., 2019; Piotrowski et al., 2005; Turkdogan et al., 1971; Turkdogan and Vinters, 1971). This sluggish reduction behavior has been suggested to be due to the slow outbound oxygen transport through the iron layer that forms around the remaining wüstite (Bonalde et al., 2005; Kim et al., 2021; Bai et al., 2022; Pineau et al., 2007; Ma et al., 2022; Ma et al., 2022; Dang et al., 2013). This is a plausible explanation because the nucleation barrier to form the cubic wüstite in the likewise cubic magnetite is very small between these two phases because the ionic oxygen lattice is the same for the two crystal structures and the interfaces between them seem to be essentially coherent. This means that the formation of wüstite inside of the magnetite proceeds essentially through local reshuffling of the iron ions, while the oxygen iron lattice remains unchanged. This leads us to the question, if the high reduction rates observed when using hydrogen instead of carbon monoxide as a reductant, might be instead related to the fast diffusion of hydrogen and not to differences in the nucleation rates or in the energetics of the reaction. The later aspect can also be ruled out as a main reason for reaction acceleration, due to the discrepancies in the underlying driving forces. This can be readily seen from the fact that the driving force for the redox reaction $FeO + CO \rightarrow Fe + CO_2$ (likewise for the other oxides) does not only exceed the one for hydrogen based reduction along the redox equation $FeO + H_2 \rightarrow Fe + H_2O$, but the former is also exothermic while the latter one is endothermic, i.e. the hydrogen-based reaction requires external heat to be added.

Similar findings about the dominance of transport over energetics when it comes to hydrogen based direct reduction were also made in atomic-scale experiments. For instance, with the recent progress in reactive and quasi-*in-situ* atom probe tomography (APT) in terms of sample preparation, reaction hub treatment and specimen workflows under maintained UHV (Ultra-high vacuum) and cryogenic conditions in conjunction with the use of labeled hydrogen (i.e. deuterium), studying the reaction process at near-atomistic scale has even become possible in experiments (Stephenson et al., 2018; Sun et al., 2021; Zhao et al., 2022; Ma et al., 2023). Using APT, El Zoka *et al.* (El-Zoka et al., 2023) observed the reduction of wüstite by deuterium at the near-atomic scale, the formation of oxygen vacancy clusters, the relationship between gangue-elements and water formation and the evolution of nano-sized pores filled with heavy water D_2O. The latter phenomena were also experimentally observed by electron diffraction and explained by phase field simulations by Zhou *et al.* (Zhou et al., 2023).

These findings and considerations suggest that the transport phenomena behind hydrogen based direct reduction seem to be critical. Irrespective of the progress sketched above, monitoring the elementary transport and reaction processes directly in real-time and at single-atomic resolution has remained challenging using experimental techniques alone, as the reduction reaction occurs at high temperatures (>873 K) and some of the rate controlling steps happen at picosecond time scales.

This has motivated the current study, namely, taking a theoretical approach at these questions. The molecular dynamics (MD) simulation approach provides a particularly suited method to studying these elementary mechanisms, capable of directly revealing the atomic interactions and ion dynamics in such a complex reactive three-component (Fe, O, H) multibody system, within the limits of the validity of the interatomic potentials being used. Moreover, the reactive force-field (ReaxFF) MD method (Ai et al., 2021; Zou and Van Duin, 2012) enables modeling chemical features of the reactions (*e.g.*, bond breaking, bond formation, charge transfer, charge state) in large-scale atomic redox systems (Van Duin et al., 2001). Based on a bond-order-based force field, it combines certain quantum mechanical potential aspects with the adiabatic Born-Oppenheimer-type Newtonian MD method for simulating kinetics (Aryanpour et al., 2010). Naturally, this method trades thermodynamic accuracy for lower computational expense, making it possible to reach simulation scales that are orders of magnitude beyond those accessible to quantum mechanical simulations. Unlike traditional force-field methods, the ReaxFF approach does not explicitly define bonds but uses bond orders to allow for continuous bond formation and breaking (Van Duin et al., 2001). It has been shown that the ReaxFF method can simulate certain reaction-critical features of redox systems, even for reactions involving transition metals, which are typically challenging to handle for classical force-field methods (Wang and Wang, 2018; Rusalev et al., 2022). Previous studies employing ReaxFF molecular dynamics have modeled the gas–solid reduction of iron oxides with limited system sizes and simulation durations (Cheng et al., 2023). These constraints primarily enabled observations of gas adsorption on the crystal surface. However, the concentration gradients of O, the penetration depth of H, and the long-time evolution of atomic neighbor relationships had not been captured in earlier works, due to system size limitations (Cheng et al., 2023; Thijs et al., 2023).

To address these challenges and more realistically capture the reduction process of iron oxides, this study employs a significantly larger system with 375 thousand atoms, representing the largest atomic-scale model used to date for this type of reduction reaction. The elementary atomistic reaction steps that occur during the reduction process of FeO exposed to molecular hydrogen at a temperature of 1273 K were investigated using ReaxFF MD simulations. The large-scale model used in this study enables the observation of some of the elementary physical–chemical processes, including the formation of near-surface oxygen gradients, the penetration behavior of hydrogen, and the stepwise reduction of the uppermost FeO regions, revealing a layered structure evolution. By extending the spatial and temporal dimensions of the simulation, our approach captures critical details such as the dynamic evolution of neighbor relationships and reaction pathways that were previously inaccessible. Combined with statistical analysis of the individual types of reaction rates, the adsorption and dissociation processes of hydrogen molecules on the surface layer of the FeO single crystal were revealed, as well as the basic steps of reducing the surface FeO layers into Fe by atomic hydrogen. With this study, we aim to provide atomistic insights into the most critical mechanisms of hydrogen-based direct reduction of iron oxides with hydrogen. Filling this knowledge gap sheds light on future strategies in leveraging mechanism-based optimization of process efficiency in terms of pellet design (*e.g.*, sintering, size, percolation, gangue, high-temperature strength, fracture toughness, and porosity), reductant gas composition (e.g., H_2, CO, CH_4, NH_3), temperature, and gas pressure. While recent studies, such as Cheng et al. (Cheng et al., 2025), have employed ReaxFF-MD to elucidate oxidation-induced microstructural evolution in Fe-based alloys, these works focused primarily on oxygen ingress and mechanical degradation during oxidation. In contrast, the present study addresses the reverse process—the reduction of wüstite (FeO) by hydrogen—providing an atomistic perspective on the early stages of green-steel production. By extending both the spatial and temporal dimensions of the simulation, our approach captures the coupled diffusion of hydrogen and oxygen ions, interfacial charge transfer, and dynamic layer-by-layer reduction mechanisms that were not accessible in previous oxidation-focused models. The diffusion coefficients reported here are effective values extracted over a fixed time window during an ongoing reactive process, and are used primarily as relative metrics for comparing species mobility rather than implying a fully steady-state transport regime.

2. Methods

2.1. Identification of the ReaxFF parameters

ReaxFF (Van Duin et al., 2001) molecular dynamics simulations were performed using the Large-scale Atomic/Molecular Massively Parallel Simulation platform LAMMPS (Plimpton, 1995). The total interaction energy can be expressed as a function of the bond orders that depend on the atomic distances (Aryanpour et al., 2010).

$E_{total} = E_{bond} + E_{over} + E_{under} + E_{val} + E_{tor} + E_{lp} + E_{H\text{-}bond} + E_{vdWaals} + E_{Coulomb}$(1)where E_{bond} represents the bond formation energies. E_{over} and E_{under} quantify the over-coordination penalty and the under-coordination penalty energy values, respectively. E_{tor} stands for the torsion angle energies. E_{lp} and $E_{H\text{-}bond}$ are the terms of lone-pair and hydrogen-bond energies, respectively. $E_{vdWaals}$ and $E_{Coulomb}$ serve to incorporate the non-bonded interactions, namely, van der Waals and Coulomb interactions, respectively. $E_{vdWaals}$ and $E_{Coulomb}$ are computed for atom pairs, while all other energy terms are calculated for the bond order between atoms *i* and *j*. This basic structure of the ReaxFF formulation offers a number of advantages but also bears some challenges. Its main advantage lies in dynamically modeling the formation and breaking of chemical bonds, a feature that provides a more nuanced understanding of reaction mechanisms and the response of materials exposed to such redox conditions, bridging the gap between traditional force fields and quantum mechanical calculations. This balance makes ReaxFF particularly valuable for studies that require a detailed yet computationally feasible analysis of complex chemical systems. The challenge of ReaxFF is the method's reliance on accurately parameterized force fields, which means that developing these parameters for new materials and reactions is complex and resource-intensive and will require machine learning methods in the future. Despite being less computationally demanding than quantum mechanical approaches, ReaxFF simulations still require significant computational resources, especially when dealing with very large systems and extended time scales, such as in this study or when aiming for extended simulation timescales. These pros and cons must be considered to develop a better understanding of the limits within which these results can be discussed.

2.2. Validation of the Shin2015 force field parameters in FeO systems

Five different reaction force field parameter sets reported in the literature (Ai et al., 2021; Aryanpour et al., 2010; Shin et al., 2015; Lu et al., 2018; Zou et al., 2012) were tested and compared to validate their ability to fit the dynamics and structure of the Fe-O system. More details can be found in the Supporting Information. The calculated radial distribution function (RDF) curves of the Fe-O bond are shown in Fig. S1(a), while the coordination number (CN) curves are provided as Fig. S1(b) to characterize the structural properties further. The main characteristics of simulating the FeO structure using individual force-field potential parameters are summarized in Table S1. Table. S2 compares the radial distribution functions of the five potential parameters with the radial distribution function curves measured by ab initio molecular dynamics (AIMD), comparing the amount of radical deviation corresponding to the peaks and the full width at half maximum (FWHM) of the curves, respectively.

Due to the limitations of the ReaxFF force-field potential parameters, the results obtained for all potential parameter sets tested show different error ranges compared with the AIMD results. When taking these errors of the resulting RDF values as main quantifies and as a basis for the selection, the Shin2015 parameters have the smallest deviation from the AIMD results and thus qualify as a suited parameter set for our purpose (deviation of r = 13.61%, FWHM = -27%). In addition, the Shin2015 parameter set shows the best match of the simulated lattice parameters to those of the main initial structures for the NaCl type structure in the temperature range of 300–1273 K. Table. S3 quantifies the lattice deformation in Fig. S2, and it can be seen that no deformation occurs along the reaction direction vertical to the surface (z). However, a more notable lattice deformation occurs in the in-plane directions x and y for different sets of potential parameters, where the Shin2015 parameter set shows the smallest lattice parameter change relative to the AIMD results at 1273 K ($\Delta x = 9.98\%$, $\Delta y = 0.98\%$) (The AIMD computational procedure reference information is given in Supporting Information S1). It is also worth noting that ongoing research in our group is focused on developing new force field parameters using machine learning approaches, which aim to address some of the limitations observed in the current parameter sets. However, the differences in parameter sets, while notable, do not critically affect the conclusions drawn in this study regarding reduction dynamics and structural evolution trends in the interface region between wustite and H_2.

Therefore, the Shin2015 potential parameters have the highest applicability for the presently studied system at a temperature range of 300–1273 K. The applicability of this parameter set to Fe-containing systems has also been tested and evaluated in previous studies (Yao et al., 2023); (Mohammadtabar et al., 2018). The results of this study, the enrichment of H atoms at the gas–solid interface and the concentration gradient of O^{2-} anions in the solid phase, are similar to those obtained from APT experiments. Due to the aberration errors associated with the APT method, where the specimen tip also serves as the imaging lens, the MD simulations of the Fe-O system can, in principle, make predictions of higher accuracy within the limits of its thermodynamic fidelity when it comes to structural aspects. When comparing the results of APT experiments and MD simulations, data normalization is achieved by Min-Max Scaler in order to compare the enrichment of H atoms at the interface and the trend of the density gradient of O atoms. Transforming each feature value to scale from 0 to 1 based on its minimum and maximum values. The Min-Max Scaler transfers the original value by:

$$X_{Scaler} = \frac{X - X_{min}}{X_{max} - X_{min}} \quad (2)$$

where X is the original value, X_{min} and X_{max} are the minimum and maximum values, respectively, and X_{Scaler} is the value after scaling.

While the Shin2015 parameters show the best overall performance among the tested ReaxFF parameter sets for this study, certain limitations should be acknowledged. One notable limitation of the Shin2015 parameter set, and ReaxFF in general, is its inability to account for magnetic effects and spin state transitions explicitly.

To further address the limitations of existing force-field parameters, a series of new machine-learning-based parameter sets tailored for the Fe-O-H system is currently under development. The results of this work are expected to be published in the near future.

2.3. Validation of Shin2015 force field parameters in γ-Fe systems

γ-Fe adopts a face-centered cubic (fcc) lattice structure, while α-Fe adopts a body-centered cubic (bcc) lattice structure. At room temperature, pure iron exists in the bcc phase (α-Fe). As the temperature reaches 1185 K, α-Fe transitions into the fcc phase (γ-Fe). In the present study, the system temperature is set at 1273 K, and the final reduction product of FeO is γ-Fe. To evaluate the applicability of the Shin2015 parameter set in simulating the γ-Fe lattice, we performed structural optimization of the γ-Fe lattice using this parameter set. Snapshots of the γ-Fe lattice before and after relaxation are shown in Fig. S3(a).

After relaxation, the γ-Fe lattice exhibits no significant distortion, with Fe atoms maintaining a well-ordered arrangement and the original fcc configuration remaining intact. Further analysis of the radial distribution function (RDF) and coordination number (CN) before and after relaxation reveals that the RDF peaks show no notable shifts and remain within the expected range. Moreover, the Fe coordination number remains stable at approximately 12 after relaxation. These results demonstrate that the Shin2015 parameter set performs well in accurately modeling the γ-Fe lattice structure.

To further evaluate the performance of the Shin2015 parameter set in simulating reaction processes within the Fe-O system, the oxidation reaction of γ-Fe in an O_2 environment was simulated (Fig. S4). As shown in the reaction snapshot (Fig. S4 (a)), the upper region of the γ-Fe lattice, where Fe atoms react with O atoms to form a mixed Fe-O solid phase, does not exhibit the expected orderly lattice transformation. Instead, this region becomes disordered. In contrast, the lower region, consisting of pure Fe, retains its lattice structure with minimal deformation.

Additionally, Fig. S4(b) presents the radial distribution function (RDF) and coordination number (CN) of the system after the reaction. These analyses reveal no significant transition indicative of an ordered lattice structure. The diffusion coefficients of 100 random O in the system were calculated in Fig. S4(c), and it can be seen that the diffusion coefficients of O within the solid-phase region (Fe lattice region) are extremely small within 10^{-11}Å^2/ps, and it is reasonable to assume that the majority of the O is stabilized within the Fe lattice after entering the lattice, and a phase transition reaction may occur. Based on these observations, we infer that the simulation discrepancies introduced by the Shin2015 parameter set primarily arise in the interactions between Fe and O atoms.

2.4. Model construction and simulation procedures

The configuration of the simulation system is shown in Fig. S5. The in-plane dimensions of the simulation box were 108.00 Å × 108.00 Å, while the spatial length normal to the reaction interface separating the solid from the gas phase was 833.36 Å. The FeO slab contained 250,000 atoms with a height of 218.507 Å, while the gas phase comprised 125,000 hydrogen atoms, equivalent to 62,500 hydrogen molecules. Based on the initial conditions (hydrogen molecule count, gas-phase volume, and temperature of 1273 K), the estimated initial hydrogen pressure is approximately 805 MPa. The simulation temperature (1273 K, i.e., 1000 °C) was chosen to represent the solid-state reduction regime relevant to gas-based direct reduction, while keeping a stable wüstite lattice for transport analysis. The resulting high initial H2 pressure is not intended to replicate industrial conditions; instead, it provides sufficient H2 number density and accelerates rare reactive events within the accessible nanosecond-scale simulation time. This value is distinct from the dynamic pressures observed during the simulation and highlights a significant difference compared to earlier nano-scale experiments, where the maximum partial pressure of H_2 rarely exceeded a few bars. In ReaxFF simulations, such extremely high-pressure conditions must often be imposed in order to achieve faster (and hence detectable) reaction rates for a limited simulation time. To eliminate finite-size/free-edge effects, periodic boundary conditions were applied in the two in-plane directions, x and y. In contrast, fixed boundary conditions were used in the z direction normal to the reaction plane. A vacuum region with a thickness of 355 Å was added below the FeO region to eliminate boundary effects in the normal direction. Before the reduction reaction, test simulations were conducted for both the NPT (at 1273 K and 1 atm) and the NVT (at 1273 K) ensembles to study the effects of these conditions on the Fe-O lattice structure (Figs. S2 and S6). It was observed that the FeO structure optimized in the NPT ensemble in the pre-processing simulation showed a stable crystal lattice structure of FeO at 1273 K. In contrast, the structure directly pre-processed in the NVT ensemble produced an incorrect amorphous FeO structure. As experiments show clear maintenance of the FeO wüstite crystal structure at this temperature, we have chosen NPT conditions for the pre-processing. More specifically, the simulated FeO crystal was pre-processed under NPT conditions at 300 K for 10 ps, and then the temperature was raised from 300 K to the target temperature of 1273 K within a time step of 10 ps under NPT ensemble conditions. Subsequently, the system was kept at a constant temperature of 1273 K for 2000 ps before hydrogen molecules were introduced to the system. The reduction reaction was then carried out under NVT ensemble conditions at a temperature of 1273 K for 1120 ps. To keep the H_2 partial pressure of the gas mixture at the top of the system constant, H_2O molecules diffusing to the top of the simulation box (~176 Å above the reaction interface) were removed every 500 steps (the time step was 0.2 fs). Visualization and post-processing of the simulation results were carried out using the software packages VMD (Humphrey et al., 1996) and Ovito (Stukowski, 2009), respectively.

3. Results

3.1. Overall reduction kinetics

Surface relaxation and sub-surface diffusion are critical phenomena during hydrogen-based direct reduction, setting the boundary conditions for the local chemical potentials that fuel the overall reaction and redox processes. Fig. 1a (the yellow rectangular box marks the interfacial spillover zone where O diffuses outward into the gas phase and H penetrates into the solid phase) shows the diffusion of H_2O molecules (redox product of the reduction reaction $FeO + H_2 \rightarrow Fe + H_2O$) from the surface into the gas phase and the intrusion of hydrogen atoms into FeO at the beginning of the reaction (10 ps) and after 1120 ps at a temperature of 1273 K. Upon reduction, surface O^{2-} anions react directly with the dissociated H atoms, departing next from the FeO surface in the form of H_2O into the gas phase. After 1120 ps, 9.9% of all O^{2-} anions were removed from the immediate outermost FeO surface layer, entering into the gas phase. Consequently, this transition region got very quickly depleted in oxygen anions, leaving the solid in a state of a non-stoichiometric Fe_nO_m (n:m > 1). This finding is interesting since after the phase diagram, the n:m ratio should be always below 1 in equilibrium, in the form of Fe_xO, with x being in the range of 0.87–0.95. This means that that the removal of oxygen anions is so fast at the surface that the ratio is deviating from this commonly assumed stoichiometry already at the beginning of the reaction, or, respectively, at the proceeding reaction interface. In either case, we refer at this point to the solid as wüstite, yet, the changing stoichiometry has to be kept in mind, for example when interpreting the state of the H agglomeration and the vacancy populations in the solid.

Simultaneously, H atoms gradually dissociate at the surface from the incoming H_2 molecules and enter into the Fe_nO_m crystal surfaces up to a depth of 85.5 Å (Fig. 1a and 1b). Free H atoms were mainly found to aggregate around the O^{2-} anions. As will be discussed in more detail below, the charge state of the H is negligible compared to O and Fe, so that Coulomb contributions to this aggregation are not so decisive and H is considered here essentially to be in an atomic state. A statistical analysis using radial distribution functions (RDF) revealed that the O-H bond length was ~1.0 Å and the Fe-H bond length was ~1.7 Å on average after 1120 ps, as shown in Fig. 1(c).

To reveal the near-surface reduction process, we calculated the corresponding overall reduction degree R emerging from these individual reaction steps (Fig. 1d), where R is defined as $R = N_t/N_0$, where N_t is the number of O^{2-} anions removed from the wüstite at an elapsed time t, and N_0 is the initial number of O^{2-} anions in the wüstite (i.e., 125,000 O^{2-} anions). With proceeding reduction, the number of O^{2-} anions in the wüstite decreases, resulting in a progressive increase in the reduction degree R (Fig. 1d). The reduction rate, i.e. the first time derivative of the reduction degree dR/dt gradually drops after the onset of the reaction (Fig. 1e). This trend agrees well with the decaying kinetics of hydrogen reduction of wüstite observed in experiments (Bonalde et al., 2005). This observation gives a first hint that the rapid build-up of a reduced Fe layer on top of the surface of the wüstite slab seems indeed to act as an elementary kinetic barrier which reduces outbound oxygen transport kinetics. This hypothesis will be discussed in more detail below.

To quantitatively elucidate the diffusion behavior of individual species in the redox system, the effective diffusion coefficients of hydrogen, oxygen, and iron were calculated based on the trajectories of randomly selected 200 atoms of each element within a time interval of 100 ps. The extraction of self-diffusion coefficients from the trajectories

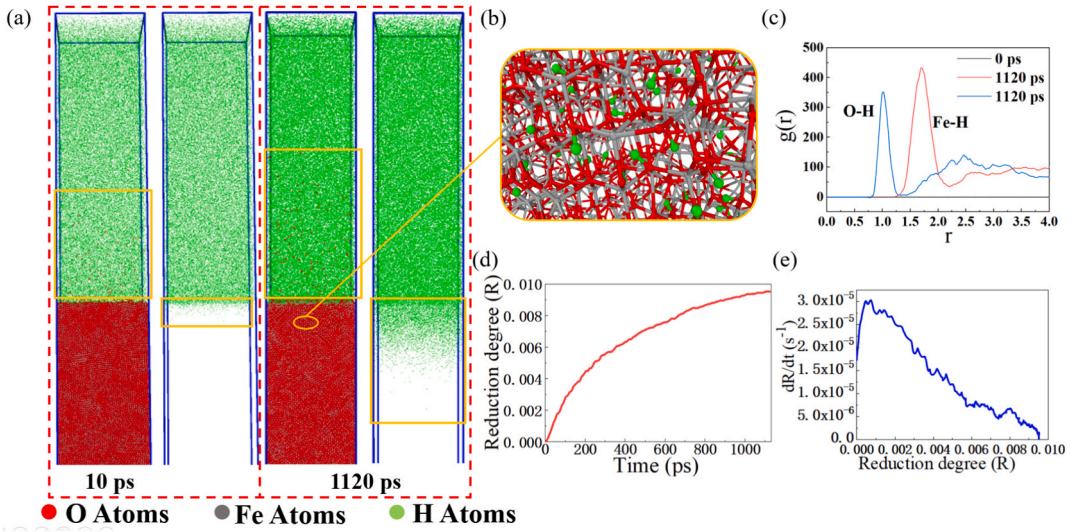

Fig. 1. Reduction behavior and kinetics during the hydrogen-based direct reduction of FeO at 1273 K. Formation of water molecules at the solid–gas interface after (a) 10 ps and 1120 ps; The yellow rectangular box in (a) highlights the interfacial spillover zone, indicating the spatial range where O atoms diffuse outward into the gas phase and H atoms penetrate inward into the solid phase. (b) Intrusion of H atoms into wüstite; (c) Radial distribution function (RDF) plots of O-H bonds and Fe-H bonds in the near-surface region (atoms in the distance of 200–225 Å from the bottom of the simulation box were analyzed) after 0 ps and 1120 ps (Note that there was no hydrogen atom in the wüstite lattice at 0 ps and thus the RDF was zero.); (d) Reduction degree R as a function of time t; (e) Corresponding reduction rate (dR/dt) vs. reduction degree (R).

(MSD-based procedure) and the construction/interpretation of the frequency histograms in Fig. 2d are detailed in Supporting Information Section S2. The spatial variation of the effective diffusion coefficient of hydrogen in the simulation box is shown in Fig. 2a. The diffusion coefficient was distinguished into three regimes based on transition regimes observed in the first derivative of the self-diffusion coefficient curve (Fig. 2b). These three regimes corresponded to the hydrogen diffusion behavior in the solid phase (region I, from 0 to 142.74 Å), solid–gas reaction interface (region II, 142.74–270.61 Å, where the first derivative of the diffusion coefficient of hydrogen reveals a positive value), and the gas phase (region III, 270.61–571.10 Å), respectively.

In the solid phase (region I), the effective diffusion coefficient of hydrogen atoms at 1273 K was less than 3 $Å^2$/ps (see Fig. 2c). Such a low diffusion coefficient was supposed to be due to adsorption of H atoms by lattice O anions. The diffusion coefficient in the interface region (region II) was mainly in the range of 0 to 200 $Å^2$/ps. In this transition region, the average value of the effective diffusion coefficient of hydrogen atoms gradually decreased from 85.62 $Å^2$/ps to 24.33 $Å^2$/ps as they entered from the gas phase into the FeO lattice. In the vicinity of the solid phase (142.74–203.85 Å in the simulation box), the diffusivity of hydrogen atoms was similar to that inside of the solid phase, with a range of 0 ~50 $Å^2$/ps. This was because hydrogen atoms were adsorbed by the O^{2-} anions in the interface region (Fig. 1b). In contrast, in the vicinity of the gas phase (203.85–270.61 Å in the simulation box), the hydrogen atoms had a large diffusion coefficient (20–200 $Å^2$/ps), similar to that in the gas phase. The large variation of the hydrogen diffusivity in the transition region (region II) could be due to the deviation of the interatomic bonding and van der Waals forces between hydrogen atoms and oxygen anions. In the gas phase (region III), the diffusion coefficient of hydrogen (in the form of a molecule) was much larger (average value of 85.62 $Å^2$/ps) compared with that in the solid phase (average value of 24.33 $Å^2$/ps). The diffusion coefficient of H in the gas phase includes hydrogen molecules and water molecules (the diffusion coefficient of water molecules is shown in Fig. S7). The diffusion coefficients of molecules in the gas-phase region are strongly influenced by pressure, temperature, and intermolecular forces, resulting in a wide range of diffusion coefficients. The calculated H diffusion coefficient at 1273 K in the Fe-O-H system was further compared with the experimental data in the Fe-H system, as no experimental data of the H diffusion coefficient at about 1273 K in the Fe-O-H system was available in the literature. It was found that the diffusion coefficient of H in ferritic stainless steel was 0.05 $Å^2$/ps at 873 K (Iacoviello et al., 1998). Jaroslav *et al.* experimentally obtained diffusion coefficients of 0.001–0.007 $Å^2$/ps for H in TRIP 800 Steel (magenta linein Fig. 2(c)) (Sojka et al., 2016). Zhou *et al.* (Zhou et al., 2021) found through simulations that at 900 K, the diffusion coefficient of H in nanocrystalline iron was 10 $Å^2$/ps (blue line in Fig. 2(c)). This comparison between these literature data and the current simulation results shows a fair consistency between calculated and experimental values, but further experiment seem to be required to explore H diffusion in iron oxides.

Fig. 2(d) shows the frequency histograms of the distribution of the simulated diffusion coefficients for each of the atomic species considered. H shows a broad distribution of its diffusion coefficients (0–300 $Å^2$/ps) in both the wüstite (as atomic H) and in the gas phase (as either H_2 and H_2O). The diffusion coefficients of most of the O anions were around 0.176 $Å^2$/ps in the wüstite phase, while the diffusion coefficient of H_2O is much larger, namely, in the range of < 1.0 $Å^2$/ps. Compared with oxygen ions (with diffusion coefficients of 0.176 $Å^2$/ps) in the solid phase, Fe ions showed larger diffusion coefficients in the range of 0–0.3 $Å^2$/ps in FeO (and the O-depleted Fe_nO_m) with a normal distribution function, Fig. 2(d). This difference may be due to the difference in ionic radius of Fe^{2+} (0.78 Å) and O^{2-} (1.4 Å) in the Fe_nO_m (including FeO) lattice (Shannon, 1976), where iron ions diffuse through the oxygen lattice. It is important to note that the diffusivity values of O and Fe ions in the solid phase are used in this study only as relative metrics under the same conditions to compare the relative ease of diffusion between different elements. In molecular dynamics simulations, the pressure inside the simulation box is set as high as 3000 atm to facilitate rapid reactions within the ps timescale, enabling the observation of atomic interactions for research purposes. Additionally, reaction products are continuously removed from the system. Therefore oxygen diffusivity obtained in this study differs significantly from experimental results under 1 atm conditions, such as the oxygen diffusivity in the solid phase during CO reduction of FeO, which is reported as $5 \times 10^{-8} Å^2$/ps. (Yamaguchi and Someno, 1982) Further experimental studies will be conducted in the future to investigate the actual diffusivity values of elements in the Fe-O-H system.

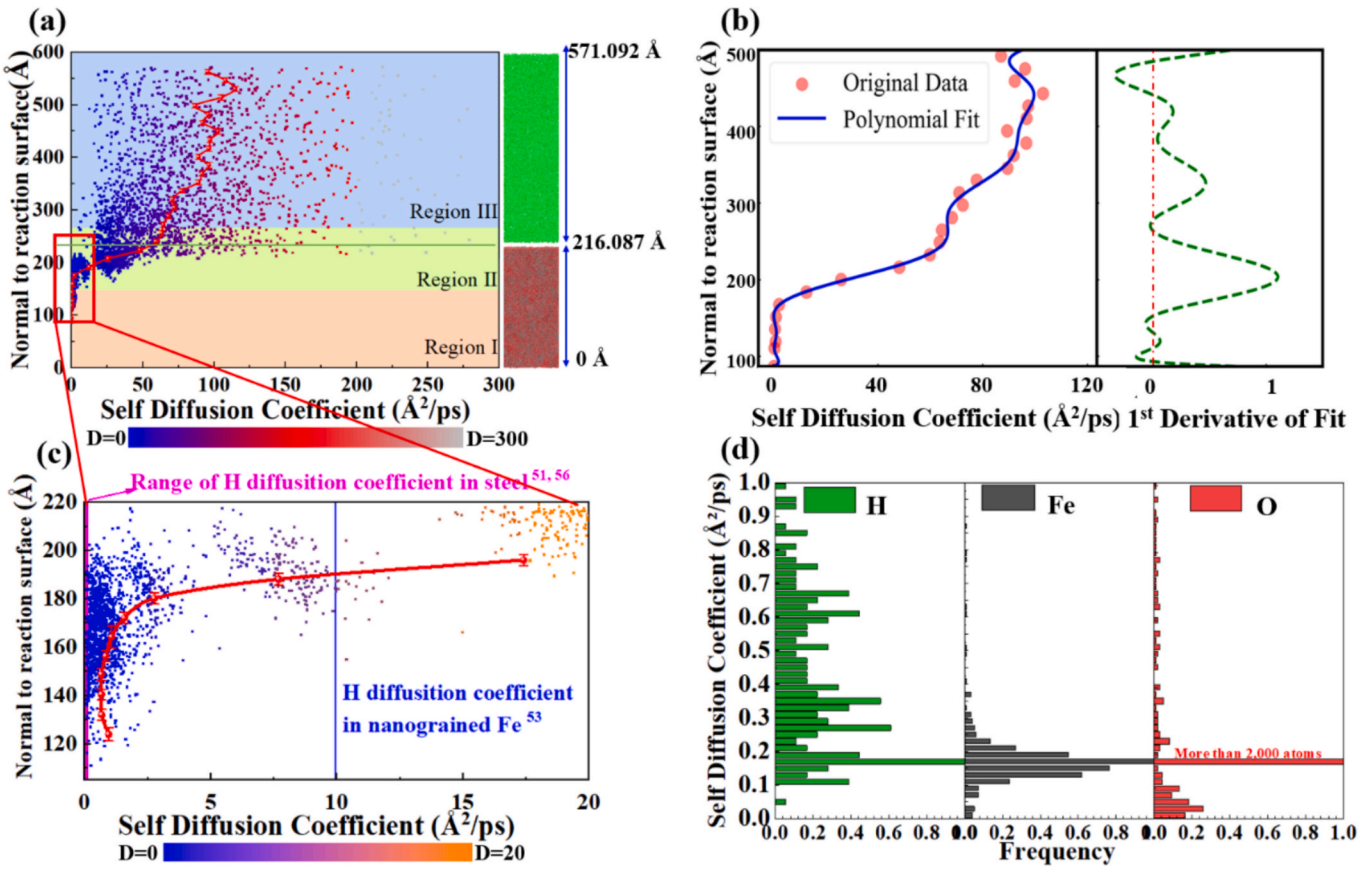

Fig. 2. Diffusion coefficients of individual species at 1273 K in the simulation box: (a) Spatial distribution of the diffusion coefficients of hydrogen. The red curve represents the average values with a binning size of 30, corresponding to a binning width of about 16 Å). (b) Spatial distribution of the average diffusion coefficients of hydrogen in 30 sub-groups along the normal direction to the reaction surface and its first-order derivative. (c) The corresponding magnified region in (b), with annotations of data in the literature. Magenta line: Measured diffusion coefficient of H atoms in stainless steel at 873 K (0.05 $Å^2$/ps) (Fukai, 1993) and in TRIP800 steel (0.001–0.007 $Å^2$/ps) (Iacoviello et al., 1998); Blue line: diffusion coefficient of H atoms in nano-grained Fe (in a body-centered cubic structure) obtained from simulations at 900 K (10 $Å^2$/ps) (Zhou et al., 2021). The red curve shows average values with a binning size of 10, corresponding to a binning width of about 9 Å. (d) Frequency histogram of the distribution of diffusion coefficients of Fe, O, and H atoms in solid phase. ("More than 2000 atoms" means that there are more than 2000O particles with a diffusion coefficient of about 0.176 $Å^2$/ps.).

3.2. *Diffusion profile of redox species across the reaction interface*

Fig. 3a displays the atomic density (number of atoms of an element in unit volume) of Fe, O, and H atoms across the gas–solid interface (200–225 Å) and the hydrogen molecular densities at 1120 ps. The hydrogen molecular density curves are realized by counting the coordination number of H atoms in the interfacial region. It can be distinctly observed in the figure that in the solid phase the H element is mainly present in the form of H atoms, and the H atoms are enriched at the interface. In the gas phase, hydrogen molecules are the main form of H element. The simulation results concurred well with the experimental observation using APT in the literature (where the sample was reduced by deuterium gas at 973 K for 5 s) (El-Zoka et al., 2023), see Fig. S8. Due to the different sizes of the MD (~200 Å) and APT (~700 Å) datasets, the absolute values of the concentration data were not compared directly. Instead, the concentration profiles of H atoms and O anions from experiments and simulations were normalized using the Min-Max normalization method (see 'Method'), as shown in Fig. 3b and 3c. The normalized hydrogen density showed a similar value of ~0.6 inside the FeO solid for both the APT measurement and the MD simulation (Fig. 3b). The interface region was enriched in H atoms, as indicated by the spike of the H density (Fig. 3b). Such enrichment can be attributed to the adsorption of H atoms on the surface-active sites of the FeO surface (where some O anions were removed during the reduction reaction). However, the experimentally measured interface with a width of 5 nm extended broader than that observed in the simulation with a width of 0.5 nm. This discrepancy was most likely due to the larger system size (70 nm for the APT measurement vs. 20 nm for the MD simulation) and longer reaction time (5 s for the APT vs. 1100 ps for the MD) in the APT experiment. Such longer exposure to hydrogen in the experiment can result in a higher reduction degree, which alters the width of the reaction interface.

During the hydrogen-based direct reduction, O was gradually removed by dissociated H_2 at the solid–gas interface, as suggested by a decrease in the density of O anions in the region close to the surface from 200 to 225 Å (relative to the density of Fe ions, Fig. 3c and Fig. S8(a)). Consequently, after 1120 ps, an O anion concentration gradient occurred in the top surface region of the FeO. Therefore, in the surface region, FeO transformed into Fe_nO_m, and the value of n:m changed from 1:1 at 0 ps to a maximum of 5:1 after 1120 ps. The overall concentration profile of oxygen revealed a sigmoid shape in both simulation and experimental results. In addition, the simulated oxygen profile showed fluctuation when the normalized oxygen density was above 70% and this fluctuating behavior disappeared when the normalized oxygen density was below 70%. Such behavior was supposed to be due to a change in the oxygen diffusion rate across the interface region. El-Zoka *et al* (El-Zoka et al., 2023). suggested several reasons: i) a change in oxygen diffusion mechanisms; ii) a change in the crystal structure of the remaining wüstite; and iii) a change in the internal point defect, line defect and/or pore structures. As pores and other macroscopic defects

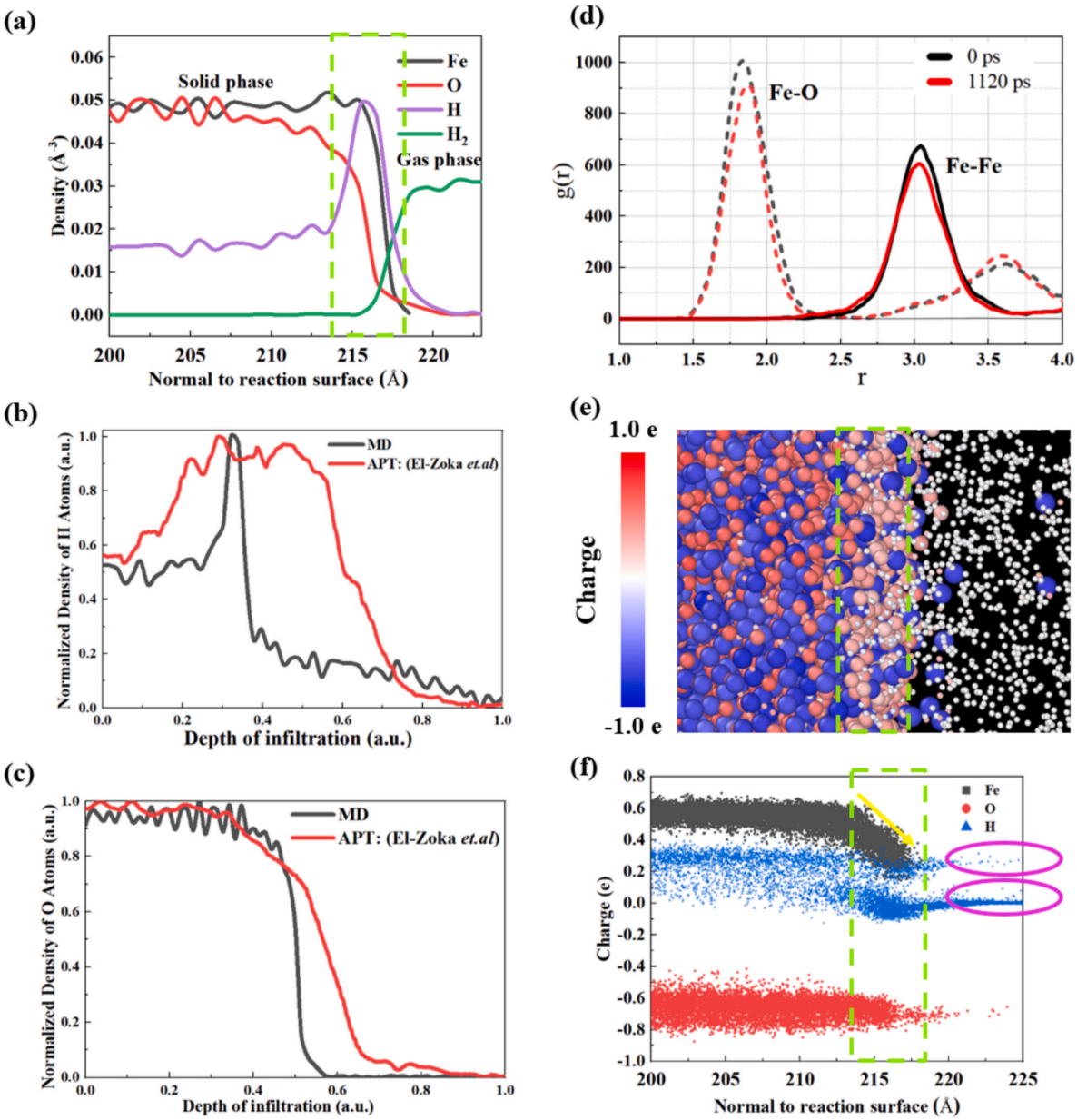

Fig. 3. Characteristics of the reduction behavior at the reaction interface (200–225 Å) during the reduction of FeO with H_2 (a) Number density of Fe, O, and H atoms at 1120 ps; Comparison of normalized distribution density of (b) H-atom and (c) O-ions measured by atom probe tomography (APT) (El-Zoka et al., 2023) and MD simulation; (d) Radial distribution function (RDF) profiles of Fe-O and Fe-Fe bonds before and after the reaction; (e) Schematic of the charge distribution of the FeO system at 1120 ps; and (f) the corresponding charge quantities of different atoms.

were not included in this simulation, this cannot affect the simulation results here. Otherwise, different shapes of oxygen profiles between the experiment and simulation are expected. As the change in the chemistry of Fe_nO_m after reduction was observed in the simulation, it is a possible reason for the change in the diffusion coefficient. Nevertheless, due to the limitations of the system scale and lattice parameters, the diffusion mechanisms of oxygen remained unexplored in this study. To better understand the underlying diffusion mechanisms requires future detailed studies using Monte Carlo simulations and first-principles calculations.

Moreover, the simulation evidenced significant penetration of H atoms into the solid phase (126.69 Å), which might be attributed to the relatively large interstitial space within the O-depleted Fe_nO_m lattice. The simulated diffusion coefficient of hydrogen atoms in the Fe_nO_m was much higher ($D_H = 0.415 \pm 0.19$ $Å^2$/ps) compared with that of oxygen anions ($D_O = 0.176 \pm 0.03$ $Å^2$/ps). This result underlines that the inward diffusion of H atoms was not the rate-limiting step during the reduction. The penetration of H atoms into the FeO lattice results in larger Fe-O bond lengths and smaller Fe-Fe bond lengths, as suggested by the RDF profiles of Fe-O and Fe-Fe bonds in the FeO lattice near the surface region (200–225 Å), Fig. 3d.

Fig. 3e shows the atomic charge distribution of the system after 1120 ps. The FeO possessed positively charged Fe ions (depicted as the red spheres), while O anions were negatively charged (represented by the blue spheres). The average charge quantity of Fe in the FeO lattice ranged from 0.4e to 0.8e, while that of O anions was from −0.8e to −0.4e, Fig. 3f. Near the surface, the Fe cations were gradually reduced to metallic Fe, and the charge quantity of Fe ions reached zero for metallic Fe. This process is due to charge transfer. The 2 electrons the of O^{2-} anions were gradually transferred to the positive charge of Fe^{2+} cations with the proceeding FeO/Fe interface, as indicated by the gradient in the peak color in Fig. 3e. Hydrogen atoms in H_2 molecules had a charge of

zero (Fig. 3e and 3f). When H atoms react with O anions to form water molecules, a slightly positive charge of H atoms was observed, as indicated by the dark pink color of the hydrogen atoms in the water molecules (Fig. 3e). Moreover, the H atoms became more positively charged as they penetrated into the solid phase and combined with O^{2-}ions in the lattice (as shown in pink color). Also, several H atoms were present in the lattice void in a free-charged state, as indicated by the white color. The average charge quantity of H atoms within the FeO crystal region ranged from 0 to 0.4 e.

The variation of the number density of O and H along the normal direction of the reaction interface was further investigated throughout the entire reaction process at 1273 K from 0 ps to 1120 ps, Fig. 4a. Details of the characterization method are summarized in Supporting Information S3. Compared with the H atoms, the O anions exhibited less fluctuation in their density. Particularly in FeO, the density of O anions remained almost unchanged. In the preceding discussion, we found that there is a concentration gradient of O^{2-} anions and a significant enrichment of H atoms in the interfacial region. The slope (K) for the atomic density gradient is defined in the following form: K = Atomic density / Distance. The absolute values of parameter K in this study reflect the diffusion potential of the atom. A smaller |K| value indicates a lower diffusion potential of atoms. Fig. 4b shows the plots of |K| values for O and H atoms in different time intervals. As the reaction progresses, the trend of |K (O)| and |K (H)| decreases, indicating an increased difficulty in the diffusion of H atoms and O anions as the reaction takes place. As the reaction proceeded, the surface FeO was reduced to Fe_nO_m, and some of the surface O left the lattice as H_2O. This led to a change in the ratio of Fe and O^{2-} anions in the surface region over time along the direction normal to the reaction interface. To further characterize the specific information of Fe_nO_m in the surface region, Fig. 4(c) illustrates the change of n/m with time along the direction normal to the reaction interface (200–225 Å). As the depth increased towards the interior, n/m approached 1 and remained relatively stable. Conversely, the surface region manifested a higher reduction degree, as suggested by a larger n/m value. (n/m ≈ 5 after 1100 ps). It is worth noting that the state of n/m≈5 is not maintained as a long-term stable configuration. This ratio represents the early stages of oxygen depletion during the reduction process, wherein no phase transition from wüstite to iron was observed. The primary limiting factors include the inability of ReaxFF simulations to account for the magnetic properties of Fe, which are crucial for accurately modeling phase transitions, and the insufficient simulation timescales to capture the complete transformation process. These limitations are further elaborated and discussed in the Discussion section.

3.3. Trajectory of atoms in the reaction process

Fig. 5 shows the trajectories of O, H, and Fe atoms during a specific period in the reaction process. A visualization of the migration of near-surface O anions within 0–118.4 ps is illustrated in Fig. 5a. The near-surface O anions required approximately 60 ps to exit from the crystal structure, which was considered to be the lag time before the reaction. Similarly, the appearance of a reaction lag phenomenon was observed in a recent experiment[15]. Once oxygen diffused to the outmost surface, it reacted with H atoms to form water vapor and diffused away from the surface. It is worth noting that the water molecules did not immediately diffuse far away from the interface. At the same time, they remained active in the vicinity of the wüstite surface and might be attracted by the surface and decomposed on the surface again. This fact indicated a reversible reaction. Previous studies have confirmed that the H bonds in surface hydroxyl groups and near-surface water molecules are more robust than those in free water (Schienbein and Blumberger, 2022). This fact means that the generated water molecules stay on the FeO surface for some time and are easily attracted by the FeO surface. The time for different O^{2-} anions to detach from the surface as water molecules is variable (e.g., selected O^{2-} anions attach to the surface for approximately 60 ps). Further studies are needed to determine the specific conditions under which detachment occurs. It is speculated that detachment may be related to the accumulation of the system energy. Fig. 5(b) shows the migration path of an H atom that penetrates the FeO crystal. Due to the massive size of the calculation system, we had to split the entire calculation time into multiple small blocks to ensure a smooth display in the visualization software. Throughout the permeation process, H atoms passed through the Fe_nO_m region on the surface, the intermediate mixing region, and the FeO region inside, and the diffusion

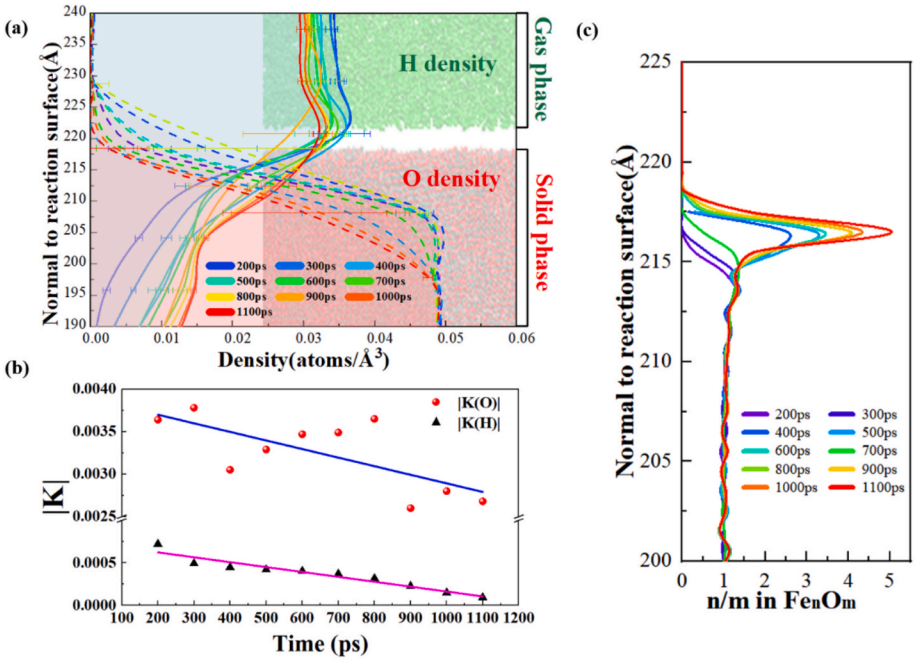

Fig. 4. (a) Evolution of the gradient of atomic density in the solid and gas phases during the entire reaction process of FeO with H_2 (Solid line: H, dashed line: O); (b) The diffusion potential (|K (O)| and |K (H)|) for different time intervals; (c) Variation curves of n/m values in FenOm in the direction of the vertical reaction interface in the surface region (200–225 Å).

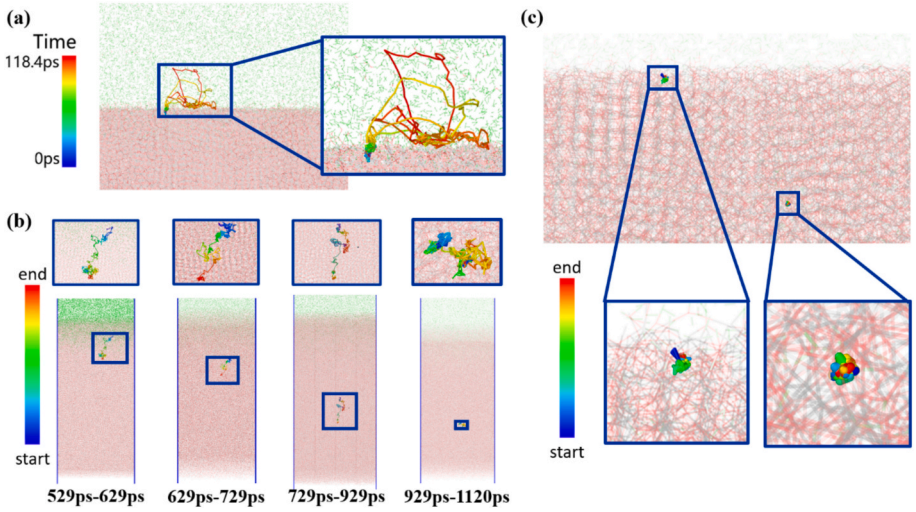

Fig. 5. Trajectory of atoms during reduction. (a) Trajectory of one oxygen atom in the interface region; (b) Trajectory of one hydrogen atom in the solid state region with different penetration depths at different times; (c) Trajectory of one iron atom in the surface region.

rate in the Fe_nO_m region is larger than that in the FeO region. It can be seen that with the elapsed time, the H atom that entered the system gradually and migrated from the surface region to the interior of the system at a max depth of about 67.8 Å after 1120 ps. However, with an increase in reaction time, it became more difficult for H to penetrate further due to the decrease in hydrogen diffusion potential as indicated by the decrease in hydrogen density gradient along the direction normal to the reaction surface (Fig. 4b). This was evidenced by a reduced traveling distance of H with elapsed time, as shown in Fig. 5(b). Furthermore, as a comparison, Fig. 5(c) shows the migration paths of two Fe ions during the reaction, and it can be seen that the Fe ions only moved around a very small region within the lattice during the entire reaction process.

4. Discussion

We conducted ReaxFF MD simulations of hydrogen reduction of FeO slab in a large system containing 375,000 atoms at 1273 K for 1120 ps. To avoid formation of amorphous FeO in the simulation, as commonly observed as a characteristic error emerging from this specific potential formulation, the structure was pre-treated under the NPT ensemble (isothermal-isobaric ensemble, a system with a constant particle number N, constant volume P and a temperature fluctuating around an equilibrium value T) before the subsequent simulation of the reaction process. According to the simulation results and under the constraints of the validity of the used potential fit, the elementary steps of the hydrogen-based reduction of FeO are summarized in Fig. 6. The first step involves the dissociation of H_2 into H atoms under the catalytic effect of the surface Fe ions that remain at the uppermost layer after the surface O^{2-} anions have reacted with H to form water molecules that were released into the gas phase (Zhang et al., 2023; Zhang et al., 2022) (Fig. 6(a), step ① and ②). Note that the H diffusion coefficient in the gas phase is not identical to that at the solid–gas interface due to mixed interfacial populations (surface-constrained H, highly mobile H in H_2/H_2O, and transient intermediates), leading to different dominant ranges (interface: ~5–50 $Å^2$/ps; gas: ~5–200 $Å^2$/ps; see Fig. 2a). Some H atoms

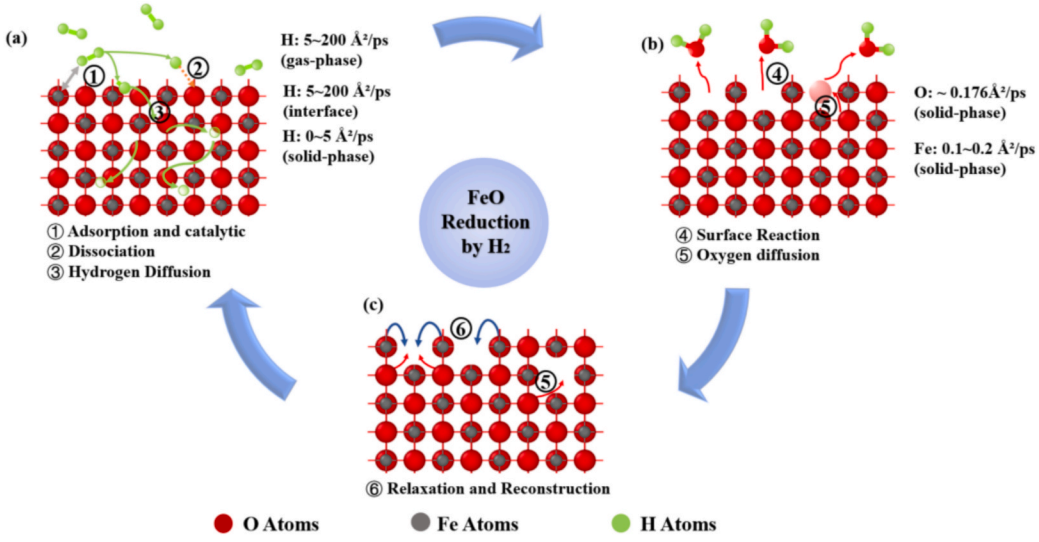

Fig. 6. Schematic mechanism of kinetic behavior for atoms during the hydrogen reduction of FeO, where the diffusion coefficients of the particles at each stage are labeled on the right side of the corresponding figure. (a) Catalytic dissociation of hydrogen molecules on the surface of FeO, adsorption and dissociation process of H atoms. (b) Reduction reaction of H and O to produce water molecules and desorption process. (c) After the surface O^{2-} anions are reduced to form lattice vacancies, the internal O^{2-} anions form a concentration difference and migrate toward the solid–gas interface and the internal lattice structure reconstruction process.

penetrate the FeO crystal lattice and migrate along the interstitial sites (see Fig. 5(b) and Fig. 6(a), step ③). This migration involves bonding and bond breaking between hydrogen atoms and oxygen ions. The bond length between H and O inside the FeO lattice is about 1.0 Å (see Fig. 1 (b) and (c)). The interstitial sweeping of the H into the FeO leads to an increase in the Fe-O bond length in the lattice. Then, dissociated H reacts with the O in the outermost surface monolayers to form OH^- intermediates (Fig. 6(a) and (b)). When these OH^- groups suspend on the surface, they attract other free H atoms in the vicinity and then desorb in the form of H_2O molecules, leaving an oxygen anion vacancy behind inside the surface Fe_nO_m monolayer (Fig. 6(b), step ④). The oxygen ions beneath migrate between the lattice vacancies and are reduced when they reach the surface (Fig. 6(b), step ⑤). The oxygen anion vacancy leads to structure relaxation or even to reconstruction features (Fig. 6(c), step ⑥). Fig. S9 shows a snapshot of the process as obtained from the simulations.

The calculated self-diffusion coefficients of hydrogen and oxygen demonstrate that the reduction rate is predominantly governed by the slower outward migration of oxygen from the solid lattice. These findings further extend beyond previous oxidation-oriented ReaxFF studies such as Cheng et al. (Cheng et al., 2025), providing an inverse perspective on the Fe–O redox process. By resolving hydrogen-driven oxygen extraction and interfacial diffusion dynamics at atomic resolution, the present work advances toward a unified mechanistic understanding of oxidation–reduction symmetry in Fe-based materials. In contrast, hydrogen diffuses rapidly thon steps only in the outermost surface regions of the FeO crystal. The simulation time was not long enough for a full metallic iron monolayer or nucleus to form. Additionally, the ReaxFF parameter set used in this study does not account for the magnetic properties of the Fe atoms and the simulated phases, which are critical for accurately describing the phase transitions that occur in this system. The magnetic transitions between ferromagnetic and antiferromagnetic states might play a pivotal role in the structural transformation from wüstite to metallic iron. This omission limits the ReaxFF framework's ability to capture the oxide-to-metal transition mechanism effectively, a topic which is therefore also outside the scope of the present study.

Moreover, the simulated physical time required to observe localized phase transitions is likely to extend to the scale of seconds. Achieving such large simulation time scales would require computational resources that are not accessible today. The crystal structures of pure iron, which depend on temperature, assume a bcc lattice below 1183 K and an fcc lattice above 1183 K during the reduction process. Indeed, these transitions were not observed in our study due to the combined constraints of simulation time and the limitations of the ReaxFF parameter set. In addition, our recent ab initio metadynamics/DFT study indicates that H2 dissociation on FeO surfaces involves a pronounced barrier (~1.03–1.38 eV), whereas the subsequent O–Fe bond breaking after O–H formation only requires a very small barrier (Jiang et al., 2025). Therefore, the "rate-determining step" inferred from atomistic simulations can be scenario-dependent: our ReaxFF-MD represents an idealized, defect-scarce interface where a locally densified near-surface Fe layer may hinder oxygen transport, while in practical experiments macro-scale porosity/cracks/defects can facilitate oxygen transport, making H_2 dissociation/activation one of the dominant rate-limiting steps. The influence of pre-existing native defects (Fe/O vacancies) and defect-assisted transport coupled with FeO–Fe phase evolution will be investigated in our ongoing AIMD-based study using more suitable electronic-structure methods; since this work is still in progress, detailed results are not included here.

5. Conclusion

In this study, we conducted reactive force field molecular dynamics (ReaxFF-MD) simulations of the reduction of a FeO slab with hydrogen at 1273 K in a system containing 375,000 atoms in ionic and molecular forms. Based on the simulation results, a detailed atomic-scale reduction model was proposed to describe the main rate-limiting reduction mechanisms associated with reducing solid FeO with molecular hydrogen H_2. This process involves the catalytic dissociation of H_2 molecules into H atoms on the FeO surface and their subsequent diffusion into the FeO lattice. H atom diffusion in FeO shows different kinetics in two regions: in the solid–gas interface region, the self-diffusion coefficient of H atoms is 20–200 $Å^2$/ps, while in the solid phase region, it is 0–5 $Å^2$/ps. Oxygen diffusion in the wüstite is extremely slow (around 0.176 $Å^2$/ps) compared with H, which is the rate-limiting step in the reaction process. The gradient of oxygen number density in the MD simulation agrees well with the trend of the curve observed in the APT experiments. It implies the success of the simulation model for the reaction behavior at the FeO-H_2 gas–solid interface. However, further improvement in the force-field potential parameters is required to simulate the phase transformation from wüstite to iron. This study provides the basis for fundamental theoretical studies of hydrogen reduction of wüstite, clarifies the diffusion coefficient of H atoms in wüstite, and explores the possible limiting links for reduction. This study compares theoretical simulation studies with experimental results to provide experience and comparative data for future research in this direction.

CRediT authorship contribution statement

Yushan Bu: Writing – original draft, Visualization, Validation, Formal analysis, Data curation. **Kejiang Li:** Writing – review & editing, Supervision, Software, Methodology, Investigation, Formal analysis, Conceptualization. **Yan Ma:** Writing – review & editing, Methodology, Conceptualization. **Zeng Liang:** Software, Investigation. **Jianliang Zhang:** Supervision, Funding acquisition. **Dierk Raabe:** Writing – review & editing, Supervision, Conceptualization.

Declaration of competing interest

The authors declare that they have no known competing financial interests or personal relationships that could have appeared to influence the work reported in this paper.

Acknowledgments

The authors acknowledge the financial support from the Young Elite Scientist Sponsorship Program by CAST (YESS20210090), Natural Science Foundation of Beijing (J210017), China Baowu Low Carbon Metallurgical Technology Innovation Fund under Grant No. 20210901, Anhui Major Industrial Innovation Program under Contract No. AHZDCYCX-LSDT2023-01. The authors acknowledge the many highly valuable and intense scientific discussions on the topic of hydrogen reduction with Joerg Neugebauer, Mira Todorova and Jaber Rezaei Mianroodi from the Max-Planck-Institut für Eisenforschung (MPIE). YM acknowledges financial support through Walter Benjamin Programme of the Deutsche Forschungsgemeinschaft (project number 468209039). DR is grateful for the financial support through the ERC Advanced grant ROC (Grant Agreement No 101054368). Views and opinions expressed are however those of the author(s) only and do not necessarily reflect those of the European Union the ERC. Neither the European Union nor the granting authority can be held responsible for them.

Appendix A. Supplementary data

Supplementary data to this article can be found online at https://doi.org/10.1016/j.ces.2026.123611.

Data availability

At the end of the manuscript, I have shared the link to my research

data.

References

Raabe, D., 2023. The Materials Science behind Sustainable Metals and Alloys. Chem. Rev. 123, 2436–2608.

Raabe, D., Tasan, C.C., Olivetti, E.A., 2019. Strategies for improving the sustainability of structural metals. Nature 575, 64–74.

IEA, World Energy Outlook 2022, in: IEA (Ed.), Paris, 2022.

Vogl, V., Åhman, M., Nilsson, L.J., 2018. Assessment of hydrogen direct reduction for fossil-free steelmaking. J. Clean. Prod. 203, 736–745.

Spreitzer, D., Schenk, J., 2019. Reduction of iron oxides with hydrogen—a review. Steel Res. Int. 90, 1900108.

Souza Filho, I.R., Springer, H., Ma, Y., Mahajan, A., da Silva, C.C., Kulse, M., Raabe, D., 2022. Green steel at its crossroads: hybrid hydrogen-based reduction of iron ores. J. Clean. Prod. 340, 130805.

Sastri, M., Viswanath, R., Viswanathan, B., 1982. Studies on the reduction of iron oxide with hydrogen. Int. J. Hydrogen Energy 7, 951–955.

Chen, Y., Zuo, H., 2021. Review of hydrogen-rich ironmaking technology in blast furnace. Ironmak. Steelmak. 48, 749–768.

IEA, Iron and Steel Technology Roadmap, in, 2020.

El-Geassy, A., Nasr, M., 1988. Influence of the original structure on the kinetics of hydrogen reduction of hematite compacts. Trans. Iron Steel Inst. Jpn. 28, 650–658.

Gallegos, N., Apecetche, M., 1988. Kinetic study of haematite reduction by hydrogen. J. Mater. Sci. 23, 451–458.

Weiss, B., Sturn, J., Winter, F., Schenk, J.L., 2009. Empirical reduction diagrams for reduction of iron ores with H2 and CO gas mixtures considering non-stoichiometries of oxide phases. Ironmak. Steelmak. 36, 212–216.

W. Zhang, J. Zhang, Q. Li, Y. He, B. Tang, M. Li, Z. Zhang, Z. Zou, Thermodynamic analyses of iron oxides redox reactions, in: Proceedings of the 8 th Pacific Rim International Congress on Advanced Materials and Processing, Springer, 2016, pp. 777–789.

Bonalde, A., Henriquez, A., Manrique, M., 2005. Kinetic analysis of the iron oxide reduction using hydrogen-carbon monoxide mixtures as reducing agent. ISIJ Int. 45, 1255–1260.

Halder, S., Fruehan, R., 2008. Reduction of iron-oxide-carbon composites: part I. Estimation of the rate constants. Metall. Mater. Trans. B 39, 784–795.

Zhang, J., Li, Y., Liu, Z., Wang, T., Wang, Y., Li, K., Wang, G., Xu, T., Zhang, Y., 2022. Isothermal kinetic analysis on reduction of solid/liquid wustite by hydrogen. Int. J. Miner. Metall. Mater. 29, 1830–1838.

Meshram, A., Korobeinikov, Y., Nogare, D.D., Zugliano, A., Govro, J., OMalley, R.J., Sridhar, S., 2023. Modeling the first hydrogen direct reduction pilot reactor for ironmaking in the usa using finite element analysis and its validation using pilot plant trial data. Processes 11, 3346.

Chen, Z., Zeilstra, C., van der Stel, J., Sietsma, J., Yang, Y., 2019. Review and data evaluation for high-temperature reduction of iron oxide particles in suspension. Ironmak. Steelmak.

Piotrowski, K., Mondal, K., Lorethova, H., Stonawski, L., Szymański, T., Wiltowski, T., 2005. Effect of gas composition on the kinetics of iron oxide reduction in a hydrogen production process. Int. J. Hydrogen Energy 30, 1543–1554.

Turkdogan, E., Olsson, R., Vinters, J., 1971. Gaseous reduction of iron oxides: Part II. Pore characteristics of iron reduced from hematite in hydrogen. Metall. Mater. Trans. B 2, 3189–3196.

Turkdogan, E., Vinters, J., 1971. Gaseous reduction of iron oxides: Part I. Reduction of hematite in hydrogen. Metall. Mater. Trans. B 2, 3175–3188.

Kim, S.-H., Zhang, X., Ma, Y., Souza Filho, I.R., Schweinar, K., Angenendt, K., Vogel, D., Stephenson, L.T., El-Zoka, A.A., Mianroodi, J.R., 2021. Influence of microstructure and atomic-scale chemistry on the direct reduction of iron ore with hydrogen at 700 C. Acta Mater. 212, 116933.

Bai, Y., Mianroodi, J.R., Ma, Y., da Silva, A.K., Svendsen, B., Raabe, D., 2022. Chemo-mechanical phase-field modeling of iron oxide reduction with hydrogen. Acta Mater. 231, 117899.

Pineau, A., Kanari, N., Gaballah, I., 2007. Kinetics of reduction of iron oxides by H2: Part II. Low temperature reduction of magnetite. Thermochim. Acta 456, 75–88.

Ma, Y., Souza Filho, I.R., Zhang, X., Nandy, S., Barriobero-Vila, P., Requena, G., Vogel, D., Rohwerder, M., Ponge, D., Springer, H., 2022. Hydrogen-based direct reduction of iron oxide at 700° C: Heterogeneity at pellet and microstructure scales. Int. J. Miner. Metall. Mater. 29, 1901–1907.

Ma, Y., Souza Filho, I.R., Bai, Y., Schenk, J., Patisson, F., Beck, A., van Bokhoven, J.A., Willinger, M.G., Li, K., D., 2022. Xie, Hierarchical nature of hydrogen-based direct reduction of iron oxides. Scr. Mater. 213, 114571.

Dang, J., Chou, K.C., Hu, X.J., Zhang, G.H., 2013. Reduction kinetics of metal oxides by hydrogen. Steel Res. Int. 84, 526–533.

Stephenson, L.T., Szczepaniak, A., Mouton, I., Rusitzka, K.A., Breen, A.J., Tezins, U., Sturm, A., Vogel, D., Chang, Y., Kontis, P., 2018. The Laplace Project: an integrated suite for preparing and transferring atom probe samples under cryogenic and UHV conditions. PLoS One 13, e0209211.

Sun, B., Lu, W., Gault, B., Ding, R., Makineni, S.K., Wan, D., Wu, C.-H., Chen, H., Ponge, D., Raabe, D., 2021. Chemical heterogeneity enhances hydrogen resistance in high-strength steels. Nat. Mater. 20, 1629–1634.

Zhao, H., Chakraborty, P., Ponge, D., Hickel, T., Sun, B., Wu, C.-H., Gault, B., Raabe, D., 2022. Hydrogen trapping and embrittlement in high-strength Al alloys. Nature 602, 437–441.

Ma, Y., Bae, J.W., Kim, S.H., Jovičević-Klug, M., Li, K., Vogel, D., Ponge, D., Rohwerder, M., Gault, B., Raabe, D., 2023. Reducing iron oxide with ammonia: a sustainable path to green steel. Adv. Sci. 2300111.

El-Zoka, A.A., Stephenson, L.T., Kim, S.H., Gault, B., Raabe, D., 2023. The fate of water in hydrogen-based iron oxide reduction. Adv. Sci. 2300626.

Zhou, X., Bai, Y., El-Zoka, A.A., Kim, S.-H., Ma, Y., Liebscher, C.H., Gault, B., Mianroodi, J.R., Dehm, G., Raabe, D., 2023. Effect of pore formation on redox-driven phase transformation. Phys. Rev. Lett. 130, 168001.

Ai, L., Huang, H., Zhou, Y., Chen, M., Lü, Y., 2021. The oxidation of Fe/Ni alloy surface with supercritical water: a ReaxFF molecular dynamics simulation. Appl. Surf. Sci. 553, 149519.

Zou, C., Van Duin, A., 2012. Investigation of complex iron surface catalytic chemistry using the ReaxFF reactive force field method. JOM 64, 1426–1437.

Van Duin, A.C., Dasgupta, S., Lorant, F., Goddard, W.A., 2001. ReaxFF: a reactive force field for hydrocarbons. Chem. A Eur. J. 105, 9396–9409.

Aryanpour, M., van Duin, A.C., Kubicki, J.D., 2010. Development of a reactive force field for iron− oxyhydroxide systems. Chem. A Eur. J. 114, 6298–6307.

Wang, J., Wang, G.-C., 2018. Promotion effect of methane activation on Cu (111) by the surface-active oxygen species: a combination of DFT and ReaxFF study. J. Phys. Chem. C 122, 17338–17346.

Rusalev, Y.V., Motseyko, A., Guda, A., Guda, S., Soldatov, A., Ter-Oganessian, N., 2022. Development of a ReaxFF potential for Au–Pd. J. Phys. Condens. Matter 35, 065901.

Cheng, Q., Conejo, A.N., Wang, Y., Zhang, J., Zheng, A., Liu, Z., 2023. Adsorption properties of hydrogen with iron oxides (FeO, Fe2O3): a ReaxFF molecular dynamics study. Comput. Mater. Sci 218, 111926.

Thijs, L.C., Kritikos, E.M., Giusti, A., Van Ende, M.-A., van Duin, A.C., Mi, X., 2023. Effect of Fe–O ReaxFF on liquid iron oxide properties derived from reactive molecular dynamics. Chem. A Eur. J. 127, 10339–10355.

Cheng, Q., Conejo, A.N., Zhang, J., Xu, Q., Wang, Y., Eckert, J., Liu, Z., Şopu, D., 2025. Effect of oxidation on mechanical properties of Fe-Ni alloys: Atomic insights from ReaxFF molecular dynamics simulations. Mater. Today Commun. 45, 112248.

Plimpton, S., 1995. Fast parallel algorithms for short-range molecular dynamics. J. Comput. Phys. 117, 1–19.

Shin, Y.K., Kwak, H., Vasenkov, A.V., Sengupta, D., Van Duin, A.C., 2015. Development of a ReaxFF reactive force field for Fe/Cr/O/S and application to oxidation of butane over a pyrite-covered Cr2O3 catalyst. ACS Catal. 5, 7226–7236.

Lu, K., Huo, C.-F., Guo, W.-P., Liu, X.-W., Zhou, Y., Peng, Q., Yang, Y., Li, Y.-W., Wen, X.-D., 2018. Development of a reactive force field for the Fe–C interaction to investigate the carburization of iron. PCCP 20, 775–783.

Zou, C., Van Duin, A.C., Sorescu, D.C., 2012. Theoretical investigation of hydrogen adsorption and dissociation on iron and iron carbide surfaces using the ReaxFF reactive force field method. Top. Catal. 55, 391–401.

Yao, L., Zhang, F., Song, Z., Zhao, X., Wang, W., Mao, Y., Sun, J., 2023. ReaxFF MD simulation of microwave catalytic pyrolysis of polypropylene over Fe catalyst for hydrogen. Fuel 340, 127550.

Mohammadtabar, K., Eder, S.J., Bedolla, P.O., Dörr, N., Martini, A., 2018. Reactive molecular dynamics simulations of thermal film growth from di-tert-butyl disulfide on an Fe (100) surface. Langmuir 34, 15681–15688.

Humphrey, W., Dalke, A., Schulten, K., 1996. VMD: visual molecular dynamics. J. Mol. Graph. 14, 33–38.

Stukowski, A., 2009. Visualization and analysis of atomistic simulation data with OVITO–the Open Visualization Tool. Model. Simul. Mater. Sci. Eng. 18, 015012.

Iacoviello, F., Galland, J., Habashi, M., 1998. A thermal outgassing method (tom) to measure the hydrogen diffusion coefficients in austenitic, austeno-ferritic and ferritic–perlitic steels. Corros. Sci. 40, 1281–1293.

Sojka, J., Váňová, P., Vodárek, V., Sozańska, M., 2016. Diffusion of hydrogen in the TRIP 800 steel. Procedia Mater. Sci. 12, 66–71.

Zhou, X.-Y., Zhu, J.-H., Wu, H.-H., 2021. Molecular dynamics studies of the grain-size dependent hydrogen diffusion coefficient of nanograined Fe. Int. J. Hydrogen Energy 46, 5842–5851.

Shannon, R.D.J., 1976. Revised effective ionic radii and systematic study of inter atomic distances in halides and chalcogenides. Acta Crystallogr. Sect. Foundat. Crystallogr. 32, 751–767.

Yamaguchi, S., Someno, M., 1982. The tracer diffusivity of oxygen in wustite and cobaltous oxide. Trans. Jpn. Inst. Metals 23, 259–266.

Y. Fukai, Hydrogen diffusion in metals, in: Defect and Diffusion Forum, Trans Tech Publ, 1993, pp. 297-304.

Schienbein, P., Blumberger, J., 2022. Nanosecond solvation dynamics of the hematite/liquid water interface at hybrid DFT accuracy using committee neural network potentials. PCCP 24.

Zhang, S., Li, K., Ma, Y., Bu, Y., Liang, Z., Yang, Z., Zhang, J., 2023. The adsorption mechanism of hydrogen on FeO crystal surfaces: a density functional theory study. Nanomaterials 13, 2051.

Zhang, S., Li, K., Ma, Y., Guo, F., Jiang, C., Liang, Z., Bu, Y., Zhang, J., 2022. Density functional studies on the atomistic structure and properties of iron oxides: a parametric study. Materials 15, 8316.

Jiang, C., Li, K., Zhang, J., Ma, Y., 2025. Green steel at atomistic scale: Ab initio simulation of surface reduction mechanism of Wüstite (FeO) by hydrogen. Appl. Surf. Sci. 698, 163031.